Physica 114B (1982) 45–58
North-Holland Publishing Company

ELECTRO-ACOUSTIC CURRENT FLUCTUATIONS IN CdS

W. WESTERA

Physics Laboratory, State University of Utrecht, Princetonplein 5, P.O. Box 80 000, 3508 TA Utrecht, The Netherlands

Received 6 January 1982

Experimental data on electro-acoustic current fluctuations, in the frequency range 500 kHz to 100 MHz, are presented for semiconducting and photoconducting CdS single crystals. The measurements were carried out under pulsed-bias conditions to avoid excessive Joule heating of the samples. The experimental results are discussed in terms of our previously published theory. The latter is based on a model where bunches of conduction electrons can be trapped and detrapped in potential troughs associated with acoustic waves which are amplified from the thermal background. The experimental current-noise spectra showed local minima which can be related to the potential-trough transit-time. These transit-time effects are not described by the theory, because it did not take space-charge into account. Apart from these effects, however, in most cases the current-noise data for both semiconducting and photoconducting samples can be described by one or two Lorentzian spectra, in accordance with the theory. In some cases, however, deviating spectra showing minima and maxima which could not be related to potential-trough transit-times were observed.

Values for the electron drift-mobility obtained from voltages marking the onset of electro-acoustic current fluctuations lie well within the range of the values published by others.

1. Introduction

If a dc electric field applied to a piezoelectric semiconducting crystal causes the carrier drift-velocity to exceed the velocity of sound, travelling acoustic waves may be amplified. The first experiments on this effect were reported in 1961 by Hutson et al. [1], who observed the amplification of injected ultrasonic waves in photoconducting CdS single crystals under pulsed-bias conditions. In addition they found that if the duration of the drift-field pulse was made somewhat longer than the round-trip transit-time for acoustic waves spontaneous growth of acoustic waves originating from the thermal background occurred. In 1962 White [2] derived an expression for the sound-amplification coefficient using a linear classical continuum description. White predicted that a maximum in the sound amplification coefficient would occur at angular frequency $\omega_m = (\omega_C \omega_D)^{1/2}$, where ω_C is the angular dielectric-relaxation frequency and ω_D is the angular carrier-diffusion frequency. For CdS the value of ω_m generally lies in the GHz-range. Furthermore White showed that the amplification of an RF acoustic wave gives rise to a corresponding RF current. Preliminary measurements of the RF components of the current in a photoconducting CdS crystal by Blötekjaer et al. [3] showed a maximum near ω_m, as predicted by White. Subsequent Brillouin-scattering studies of the growth of the acoustic flux in CdS [4, 5], have shown that White's theory only applied in the weak-flux limit. With increasing acoustic flux intensities many nonlinear effects have been observed [4, 5]. These effects may include parametric generation of subharmonics, current oscillations, current saturation, current fluctuations, travelling electro-acoustic domain formation, and so on.

The first systematic measurements of electro-acoustic current fluctuations in CdS were reported by Moore [6]. Experimental data in the frequency range 1.5 MHz to 900 MHz did not show a maximum in the current-noise spectrum; instead, the noise spectrum turned out to be flat at low frequencies, and to decrease approximately as $1/f^2$ at high frequencies. This type

0378-4363/82/0000–0000/$02.75

of current noise cannot be described by a linear theory. Moore avoided the need to use nonlinear equations in that he suggested that the observed current fluctuations are caused by the trapping of bunches of free charge carriers in potential troughs, associated with the amplified acoustic waves. Assuming that the creation and annihilation of potential troughs occurs at random throughout the crystal, Moore found that the observed current fluctuations can be described by a trough creation–annihilation process. The thus obtained expression for the noise spectrum gave a reasonable explanation for his experimental data. Additional experimental results of current-noise measurements have been reported by Baibakov [7] in CdSe and by Gielen and Zijlstra [8, 9] in CdS. Moreover, Schulz et al. [10, 11] observed this trapping noise in GaAs, although their attention was mainly focussed on the parametric generation of subharmonic frequencies in the RF current.

In 1978 Zijlstra and Gielen [12] modified Moore's calculation by accounting for transit-time effects in a local description. Since, however, the boundary conditions they used imply an internal inconsistency at low frequencies their results should be considered doubtful.

In [13] we extended this local description by introducing two types of potential troughs, related to forward-travelling (i.e. towards the anode) and backward-travelling (i.e. towards the cathode) acoustic waves, respectively. The backward-travelling potential troughs were introduced to remove an inconsistency which arises when the relaxation time obtained from the current-noise spectrum is compared with that obtained from the ac impedance (cf. [14]). It was assumed that space charge, diffusion and the dielectric displacement current can be neglected, and that the kinetics of the two types of troughs are statistically independent. Furthermore the crystal anisotropy was taken into account, and consistent boundary conditions were applied. If the spontaneous fluctuations in the potential-trough creation and annihilation rates are assumed to be statistically independent, the current-noise spectrum can be described by two Lorentzian components.

The aim of this paper is to compare experimental current-noise data for photoconducting and semiconducting CdS with the calculations given in [13]. A summary of the results of these calculations is given in section 2, the experimental arrangement is described in section 3, and experimental results are presented and discussed in section 4.

2. Theory

In this section we shall summarize the results of the calculation of the spectral current-noise intensity as given in [13].

Consider an n-type homogeneous piezoelectric semiconducting crystal where the electric field is applied along a symmetry axis, the x_3-axis. In the case of CdS the x_3-axis coincides with the c-axis. Together with the x_1- and x_2-axis the x_3-axis forms a Cartesian coordinate system. The sample is supplied with ohmic contacts at $x_3 = 0$ (cathode) and $x_3 = L$ (anode). If the drift velocity of the electrons exceeds the sound velocity, acoustic waves, originating from the thermal background and travelling in the direction of the drifting electrons, are amplified. As a result potential troughs which propagate with the velocity of sound are spontaneously created and annihilated throughout the crystal. Note that the creation and annihilation occurs at random because of the incoherent nature of the thermal background waves. The electro-acoustic current fluctuations are thought to be caused by the sudden trapping and detrapping of whole groups of free charge-carriers in these potential troughs. If charge-carriers become trapped in these potential troughs, their velocity is changed from the drift velocity to the trough velocity. We have assumed that two types of potential troughs occur: one type of trough is associated with acoustic waves travelling towards the anode

(forwards) and the second type with waves travelling towards the cathode (backwards). The two types of troughs, having opposite velocity components, v_{g_3} and $-v_{g_3}$ respectively, along the x_3-axis, have been assumed to be statistically independent. In [14] we showed that the trough velocity v_g can be associated with the group velocity of the acoustic waves. As a result of the elastic anisotropy in CdS the direction and magnitude of the group velocity may differ considerably from the direction and magnitude of the acoustic phase velocity. For reasons of simplicity we neglected space-charge, and assumed that each forward-travelling trough contains N_1 electrons, and each backward-travelling trough contains N_2 electrons, where N_1 and N_2 are independent of x_3. In addition we neglected diffusion and the displacement current.

The current noise was calculated with the Langevin method. Spontaneous fluctuations in the potential-trough creation and annihilation rates were used as Langevin source-functions. On the assumption that the spatial correlation for each Langevin source-function can be described by a delta-function, we found the following expression for the spectral current-noise intensity S_I:

$$S_I(f) = 4qN_1(q\bar{n}_{s_1}v_{g_3}A)\left(\frac{\bar{v}_{d_3}-v_{g_3}}{v_{g_3}}\right)^2\frac{\tau_1/\tau_t}{1+\omega^2\tau_1^2} + 4qN_2(q\bar{n}_{s_2}v_{g_3}A)\left(\frac{\bar{v}_{d_3}+v_{g_3}}{v_{g_3}}\right)^2\frac{\tau_2/\tau_t}{1+\omega^2\tau_2^2}, \quad (1)$$

where $-q$ is the electron charge, A is the contact area, ω is the angular frequency, $f = \omega/2\pi$ is the frequency, $\bar{n}_{s_1}$, $\bar{n}_{s_2}$ are the time-averaged local densities of electrons, trapped in forward- and backward-travelling troughs, respectively, τ_1, τ_2 the mean lifetimes of the fluctuations in the numbers of forward- and backward-travelling troughs, respectively, $\tau_t = L/v_{g_3}$ is the potential-trough transit-time, and $\bar{v}_{d_3}$ is the time-averaged drift-velocity component along the x_3-axis. As a consequence of the assumption of space-charge neutrality in the steady state, $\bar{v}_{d_3}$ can be related directly to the applied voltage $\bar{V}$ by

$$\bar{v}_{d_3} = \mu_{33}\,\bar{V}/L, \quad (2)$$

where μ_{33} is an element of the mobility tensor.

As we pointed out in [13] the threshold voltage V_c for the amplification of sound waves is determined by the phase velocity $v_s(0)$ of on-axis waves:

$$V_c = \frac{v_s(0)L}{\mu_{33}}. \quad (3)$$

As a final result of the calculations given in [13] we mention the occurrence of maxima in the ac impedance at frequencies that are related to the potential-trough transit-time. These resonance frequencies are given by

$$f = f_l = \frac{(2l+1)}{2}\tau_t^{-1}; \qquad l = 0, 1, 2, 3, . \quad (4)$$

3. Experimental arrangement

For our measurements we used semiconducting and photoconducting single crystals of hexagonal n-type CdS, obtained from Eagle Picher Industries, Inc.

So that Brillouin-scattering experiments could possibly be carried out at a later stage we polished some of the crystal side-faces mechanically to a flatness of $\frac{1}{4}\mu$m. In some cases the two contact faces were also polished to a flatness of $\frac{1}{4}\mu$m. Unpolished surfaces, being several orders of magnitude less flat than polished ones, can be expected to cause considerable acoustic scattering losses, since the wavelengths of the amplified acoustic waves having frequencies around 1 GHz are about 2 μm [2, 4].

The samples were supplied with two In-evaporated ohmic contacts in such a way that the applied electric field was orientated along the c-axis (the longitudinal configuration). The In-contacts covered the end-surfaces completely. For details we refer to [14].

The dimensions, dark-conductivity at room temperature and surface characteristics of the semiconducting (s) and photoconducting (p) CdS crystals are listed in table I. Data on current saturation and ac impedances for these samples have been presented in [14]. All measurements were carried out at room temperature.

To control the conductivity of photoconducting crystals the samples were illuminated from the side with filtered light from a quartz–halogen lamp or with light from a krypton laser. The optical wavelengths were such that no band-to-band transitions were induced but carriers from local centres were generated. Therefore the absorption coefficient of the light was small and it can be assumed that the samples were homogeneously illuminated.

To avoid excessive Joule heating of the samples the high voltage was applied in pulses of 40 μs at a repetition rate of 4 Hz. The duration of these pulses was sufficient for the samples to reach a stationary state. In addition, a room temperature nitrogen or air flow was made to pass over the sample during operation.

The height of the voltage pulses was measured with a sample-and-hold circuit.

The experimental set-up for the current-noise measurements under pulsed-bias conditions is shown in fig. 1. Voltage pulses from the pulse generator, which passed through a low-pass filter to suppress higher harmonics of the pulses, were fed into an RF coaxial 50 Ω power termination. The CdS crystal (impedance Z) in series with a 50 Ω termination were connected in parallel. (The value of $|Z|$ was always much larger than 50 Ω.) The current fluctuations generated by the electro-acoustic effect developed voltage fluctuations across the latter 50 Ω resistor. Our noise-measuring circuit, which performed the frequency selection and noise-power measurement, was made up of several components. The input impedance of this circuit was approximately 50 Ω. The high-pass filter served to separate the dc part of the pulse from the ac part. It should be noted that the voltage fluctuations to be analyzed had typical amplitudes of a few microvolts, whereas the transient voltages at the input of the noise-measuring circuit were several volts. Therefore, to prevent overloading the amplifiers we used an electronically-controlled RF gate (gate 1 in fig. 1), which transmitted the noise signal only between 5 μs and 35 μs after the onset of the voltage pulse. Subsequently the noise signal was amplified and fed into an HP 8558 B spectrum analyzer. Since the power detector of the spectrum analyzer could not be used under pulsed-bias conditions, the intermediate-frequency output of the spectrum analyzer (21.4 MHz) was fed into a power meter consisting of an HP 435 A and an HP 8484 A. In

Table I
Characteristics of the semiconducting (s) and photoconducting (p) CdS samples

Sample	L (mm)	A (mm^2)	Dark-conductivity (Ω^{-1}m^{-1})	Polished faces (mm^2)
s_1	1.76	1.24×0.55	6.6×10^{-1}	–
s_2	1.84	1.27×0.59	5.6×10^{-1}	–
s_3	1.63	1.78×0.48	9.5×10^{-1}	1.78×1.63-face 1.78×0.48-face
s_4	1.76	1.24×0.43	6.6×10^{-1}	1.76×1.24-face
s_5	2.79	1.43×0.37	2.3	all faces
s_6	1.76	2.53×0.97	1.3	–
p_1	1.65	2.14×2.20	2.3×10^{-3}	–
p_2	1.14	1.81×0.76	5.5×10^{-1}	–

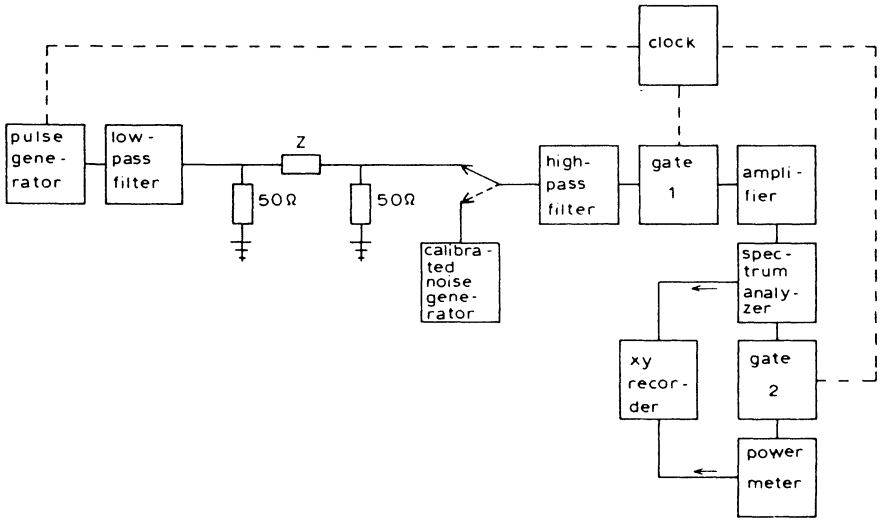

Fig. 1. Experimental set-up for measuring the spectral current-noise intensity under pulsed bias conditions.

this way the spectrum analyzer served only as a frequency band-filter and a mixer. A second gate (gate 2 in fig. 1) was used to remove the (amplified) transients from the first gate (gate 1). The gate width of the former was slightly below 30 μs. The gates and the pulse generator were synchronised by the clock.

To determine the spectral current-noise intensity S_I we measured the power P_1 of the voltage fluctuations with bias applied to the sample, and the power P_2 without bias. This background power P_2 was caused by the noise of our measuring circuit. To calibrate the measured noise power a calibrated noise generator was connected to the noise-measuring circuit (cf. fig. 1). In addition we measured P_3 (noise generator connected) and P_4 (noise generator connected, but with zero output). In can be shown [8, 9] that under these conditions the spectral current-noise intensity S_I is given by

$$S_I = \frac{P_1 - P_2}{P_3 - P_4} S_{I_0}, \tag{5}$$

where S_{I_0} is the known spectral current-noise intensity of the calibrated noise generator (output resistance 50 Ω).

With the help of calibrated attenuators we verified that during the measurements the power-meter deflection was always linearly related to the input noise.

The pulse length of 40 μs determined a fundamental low-frequency limit for the current-noise measurements. This limit turned out to be about 500 kHz. The high-frequency limit was found to be about 100 MHz. This value was due to the electrical components in the low-pass and high-pass filters, and in some cases to parasitic capacitances parallel to Z. The bandwidth of the spectrum analyzer was set at 300 kHz at low frequencies ($\leqslant$10 MHz) and at 1 MHz at high frequencies ($\geqslant$10 MHz).

The selected frequency of the spectrum analyzer could be swept automatically. Therefore, frequency-swept noise measurements were possible. The power-meter deflection and the horizontal output of the spectrum analyzer (a measure for the operating frequency) were connected to an XY-recorder. The power-meter deflections P_1, P_2, P_3 and P_4 were recorded successively with frequency-sweep times varying between 500 and 1000 s.

With the procedure described above the spectral current-noise intensity S_I could be deter-

mined with an inaccuracy of about 10%. The lowest spectral current-noise intensity detectable was approximately 5×10^{-21} A^2 s.

4. Experimental results and discussion

In this section we present and discuss the experimental results for semiconducting CdS (section 4.1) and photoconducting CdS (section 4.2). In section 4.3 electron drift-mobility values obtained from the voltages V_c marking the onset of electro-acoustic current fluctuations are compared with values from the literature.

4.1. Semiconducting CdS

The spectral current-noise intensity S_I as measured at 10 MHz as a function of applied bias voltage $\bar{V}$ is shown in fig. 2 for samples s_5 and s_6. The bandwidth for these measurements was 300 kHz. The solid lines have been drawn to guide the eye.

For sample s_6 we find that at low voltages, in fact at voltages where the current–voltage (IV–) characteristic is still ohmic, S_I increases proportionally to $\bar{V}^2$. This noise can be associated with generation–recombination noise [8, 9]. At a certain voltage V_c, S_I increases very strongly due to the occurrence of electro-acoustic current fluctuations. Since the critical voltage V_c is closely related to the threshold voltage for electro-acoustic amplification, the strong increase in the current noise allows an accurate determination of this threshold voltage [6]. In fact, the threshold voltage can be determined much more accurately from the onset of the strong current noise than from the onset of current saturation. Moreover, in general the value of the latter is found to be somewhat higher than that of the former [8]. With increasing voltage we observe a decrease in the current noise. This is contrary to the results of Moore [6], who found experimentally $S_I \sim (\bar{V} - V_c)^2$, in accordance with his theoretical model. Gielen and Zijlstra [8, 9]

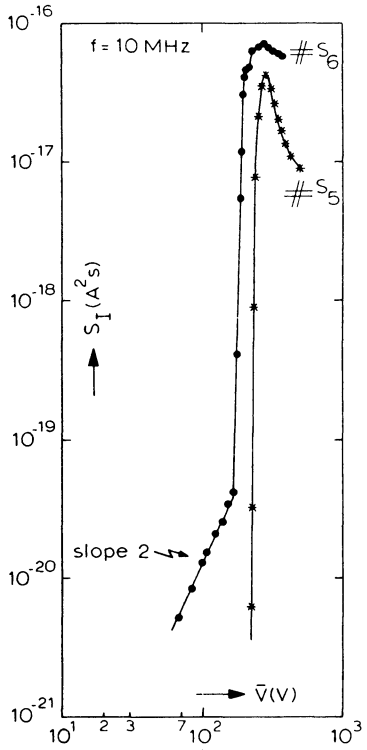

Fig. 2. The spectral current-noise intensity at 10 MHz versus applied voltage for samples s_5 and s_6. The solid lines have been drawn to guide the eye.

compared their experimental data with calculations given by Zijlstra and Gielen [12], which predicted $S_I \sim (\bar{V} - V_c)^2$ as well, at voltages well above the curvature in the IV-characteristic (in our samples $(\bar{V} - V_c)/V_c \gtrsim 0.5$). Their experimental data showed $S_I \sim (\bar{V} - V_c)^m$ with m varying between 1.6 and 4.0. Since, however, the electrical contacts on their CdS platelets covered only a small part of the crystal end-faces, the assumption of a homogeneous electric field strength was probably invalidated by the existence of stray electric fields in the fringe area. So far we have no explanation for the discrepancy between our data and those of Moore [6].

As can be seen from fig. 2 the behaviour of sample s_5 above V_c is similar to that of sample s_6. For sample s_5, however, no generation-recombination noise could be observed.

Upon inspection of eq. (1) we can conclude

that in general the voltage dependence of S_I will be very complex because of the voltage dependences of the parameters N_1, N_2, v_{g_3}, $\bar{v}_{d_3}$, τ_1, τ_2, $\bar{n}_{s_1}$ and $\bar{n}_{s_2}$.

Fig. 3 shows the spectral current-noise intensity at 10 MHz plotted versus the reduced voltage $(\bar{V}-V_c)/V_c$ for samples s_1, s_2 and s_3. At voltages slightly above V_c, S_I is approximately proportional to $(\bar{V}-V_c)^2$. With increasing voltage, however, substantial deviations from a quadratic relationship are again observed. It should be noted that the data for $(\bar{V}-V_c)/V_c$ below 10^{-1} may be quite inaccurate due to the fact that V_c could not be determined very accurately. Therefore, the errors in $(\bar{V}-V_c)/V_c$, as indicated in fig. 3, will be systematic rather than accidental.

Fig. 4 shows a current-noise spectrum for sample s_2. The experimental data are represented by black squares. Apparently these data cannot be described by a single Lorentzian, although such a shape was predicted in [6]. At low frequencies the noise spectrum shows some structure, which is not described by the theoretical expression for the current noise (eq. (1)). Structure appearing in the ac impedance measured under the same conditions was predicted theoretically [13] and can be ascribed to potential-trough transit-time effects. Maxima in the ac impedance occur at frequencies given by eq. (4). The vertical arrows in fig. 4 correspond to these resonance frequencies as obtained from the ac-impedance data. From fig. 4 we conclude that maxima in the ac impedance correspond to minima in the current noise. It should be noted that such transit-time effects in the expression for the ac impedance are only found if space charge is taken into account. However, for reasons of simplicity we neglected space charge in our calculation of the current noise [13]. Therefore no transit-time effects are included in our expression for the current noise (eq. (1)). We conclude that the structure observed in the current-noise spectrum is also caused by potential-trough transit-time effects. We expect that it will be possible to describe the current noise apart from the structure by eq. (1). The most accurate way to determine the resonance frequencies (cf. eq. (4))

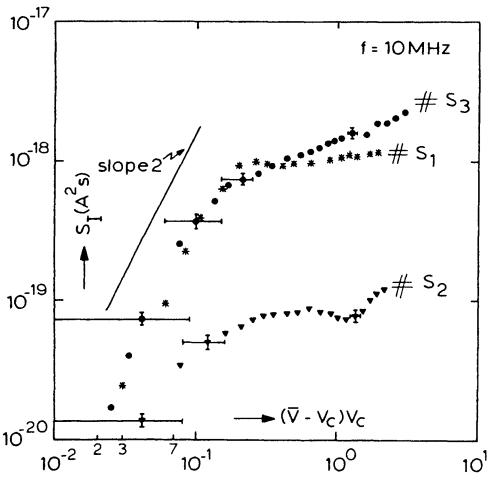

Fig. 3. The spectral current-noise intensity at 10 MHz versus $(\bar{V}-V_c)/V_c$ for several samples. The solid line represents a line with slope 2.

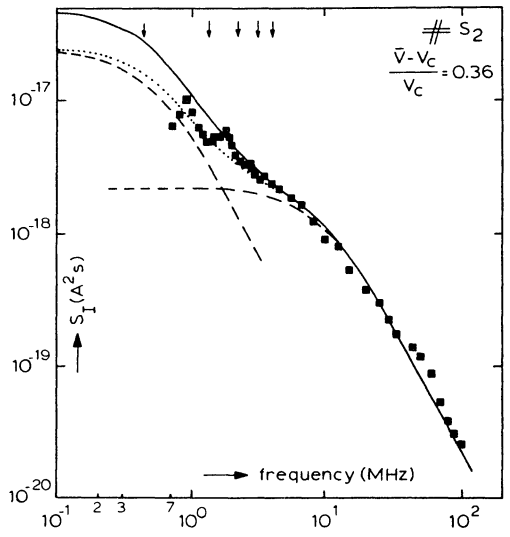

Fig. 4. Spectral current-noise intensity for sample s_2 at $(\bar{V}-V_c)/V_c = 0.36$. Black squares represent the experimental data. The solid line and dotted line have been calculated with eq. (1). The parameters used are listed in table A.1 (appendix). The dashed lines represent the separate contributions made by the single Lorentzian spectra occurring in eq. (1) to the dotted line. The vertical arrows correspond to maxima in the ac impedance.

is to use the ac-impedance data, because the bandwidth in the measurements of the current-noise spectra is finite.

Moore [6], who used a nonlocal description, in terms of total numbers of free and trapped carriers, accounted for transit-time effects in an ad hoc manner by using an expression for the autocorrelation function of the current fluctuations, originally derived by Hill et al. [15] for the case of ambipolar carrier drift. In the transit-time-dominated case Moore's calculation yielded a noise spectrum of the form $(\sin(X)/X)^2$ where $X = \frac{1}{2}\omega\tau_t$; this in turn yields minima at frequencies that are multiples of $1/\tau_t$ and maxima at frequencies given by eq. (4). Moore's experimental data, however, showed no distinct transit-time effects. Fig. 4 demonstrates that Moore's expression for the transit-time effects cannot be correct, because the positions of experimental minima and maxima are precisely the reverse of Moore's. The only correct way to account for transit-time effects is to calculate the current noise in a local description without assuming space-charge neutrality. So far no such calculation has been published.

It was not possible to fit eq. (1) directly to the current-noise data by adjusting τ_1, τ_2 and the plateau values. Therefore we used the following procedure to fit eq. (1) to the data in fig. 4. We estimated a relaxation time (the smaller of the two) from the noise spectrum and we fitted the expression for the ac impedance to the experimental ac-impedance data by adjusting the other relaxation time [14]. Subsequently we adjusted the plateau values of the Lorentzians in eq. (1) to the current-noise data with a least-squares fitting procedure. From the ac-impedance data it follows that τ_2 is always much smaller than τ_1 [14].

The numbers of electrons, N_1 and N_2, per trough can be determined from the adjusted plateau values, because $\bar{n}_{s_1}$ and $\bar{n}_{s_2}$ can be calculated from the ac impedance and the IV-characteristic [14], v_{g_3} is known from the resonance frequencies in the ac impedance (cf. eq. (4)), and $\bar{v}_{d_3}$, or rather μ_{33}, is known from V_c (cf. eq. (3)). Although the value of τ_1 as found from the ac impedance is rather inaccurate [14], the procedure described above proved to give acceptable fits.

The solid line in fig. 4 shows the result of the fitting procedure. Here, at low frequencies it is only the current-noise data at the local maxima which have been used in the fitting procedure. From this fit we obtained $N_1 \simeq 1.3 \times 10^5$, $N_2 \simeq 1.6 \times 10^4$, $\tau_1 \simeq 3.1 \times 10^{-7}$ s and $\tau_2 \simeq 1.6 \times 10^{-8}$ s. The parameters used are listed in table A.1 (appendix). It should be noted that the numerical values of N_1, N_2, τ_1 and τ_2 suggest a higher accuracy than can be obtained with the available experimental data. First of all, in most cases τ_1 cannot be obtained very accurately from the ac-impedance data [14]; in the second place at low frequencies the Lorentzian spectra are concealed by the transit-time resonances; in addition at low frequencies the magnitudes of the selected frequencies become comparable with the magnitude of the bandwidth (300 kHz) of our measuring circuit; there is a lack of data at low frequencies; lastly, since no expression for the transit-time resonances has been derived we are not sure whether in our fitting procedure we should use the data at the local maxima, those at the local minima, or even those in between. Therefore we adjusted the plateau values again, this time using all experimental data occurring in fig. 4. The dotted line in fig. 4 represents the result of this fitting procedure. The dashed lines show the separate contributions of the two single Lorentzian spectra. We found $N_1 \simeq 6.5 \times 10^4$ and $N_2 \simeq 1.8 \times 10^4$. The parameters used for this calculation are listed in table A.1 (appendix).

From further investigations we estimated the error in τ_2 to be about 20%, in τ_1 about 50% [14], in N_2 about 30% and in N_1 about 100%. We conclude that the numerical values of the parameters τ_1, N_1 and N_2 obtained from the fitting procedure are indicative only of the order of magnitude.

Fig. 5 shows the current-noise spectrum of sample s_4 at $(\bar{V} - V_c)/V_c = 0.35$. The solid line

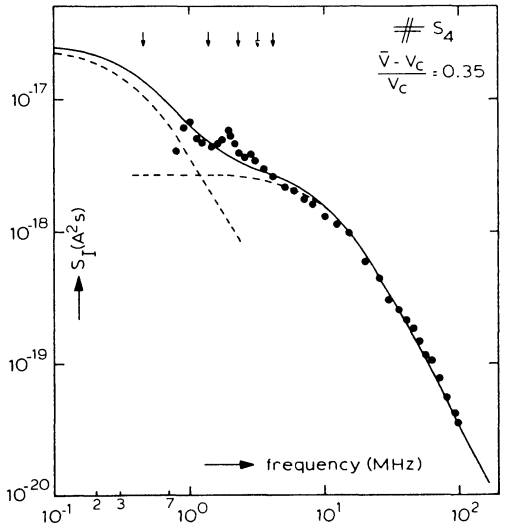

Fig. 5. Spectral current-noise intensity of sample s_4 at $(\bar{V}-V_c)/V_c = 0.35$. The black dots represent the experimental data. The solid line has been calculated with eq. (1). The parameters used are listed in table A.1 (appendix). The separate contributions of the Lorentzians in eq. (1) are indicated by the dashed lines. The vertical arrows correspond to maxima in the ac impedance.

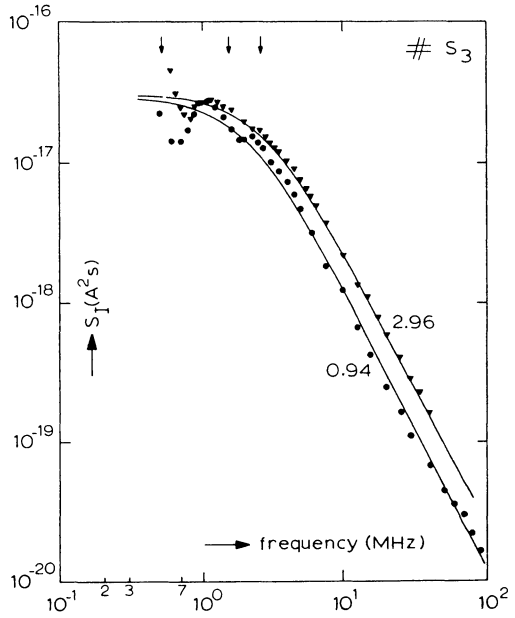

Fig. 6. Spectral current-noise intensity of sample s_3 at two different applied voltages. The values of $(\bar{V}-V_c)/V_c$ are indicated. The solid lines represent hand-fitted Lorentzian spectra. The parameters used are listed in table A.1 (appendix). The vertical arrows correspond to maxima in the ac impedance.

has been calculated with the help of eq. (1), using all experimental data. For details we refer to table A.1 (appendix). From figs. 4 and 5 we conclude that expression (1) can be fitted quite reasonably to the experimental current-noise data, apart from the transit-time resonances. Noise spectra of similar shape were obtained for sample s_1.

In some cases the current-noise spectrum is dominated by one Lorentzian spectrum in the frequency range considered. Fig. 6 shows such current-noise spectra for sample s_3 at two different applied voltages. The solid lines represent hand-fitted Lorentzian spectra. Here, again we used all experimental data. From these curves we obtained $N_2 \simeq 2\times 10^4$ at $(\bar{V}-V_c)/V_c = 0.94$ and $N_2 \simeq 5\times 10^3$ at $(\bar{V}-V_c)/V_c = 2.96$. It is observed that an increase in the applied bias voltage hardly affects the current-noise spectrum for this sample. Only a slight broadening of the noise spectrum and a decrease of the transit-time effects are observed. The relatively low value of the roll-off frequency (i.e. $(2\pi\tau_2)^{-1}$) compared to the values obtained in figs. 4 and 5, cannot be related to the fact that the contact surfaces of sample s_3 have been polished, because similar small roll-off frequencies were observed for unpolished samples (cf. fig. 7). Since the creation and annihilation of potential troughs are closely related to the spatial, angular and frequency distributions of the acoustic energy, and to the dispersion of the acoustic waves, the magnitude of the relaxation times will be mainly determined by the geometrical conditions for each sample. Manifest structure in the current-noise spectra resulting from polished end-surfaces, as reported by Gielen and Zijlstra [8, 9], was not observed in our case.

In some cases, however, the shapes of the noise spectra differed considerably from those of the noise spectra discussed previously. Fig. 7 shows spectra of sample s_6 at two different ap-

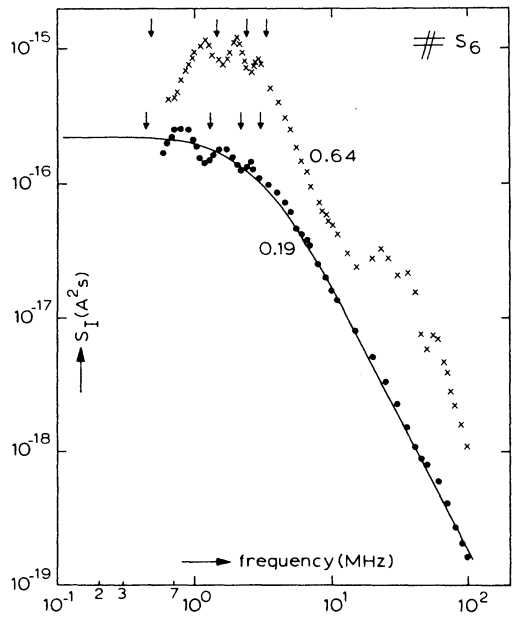

Fig. 7. The spectral current-noise intensity of sample s_6 at two different applied voltages. The values for $(\bar{V} - V_c)/V_c$ are indicated. The arrows correspond to maxima in the ac impedance. The solid line represents a hand-fitted Lorentzian spectrum. Details are listed in table A.1 (appendix).

plied voltages. At $(\bar{V} - V_c)/V_c = 0.19$ the spectrum apart from the transit-time resonances, can be described by a single Lorentzian spectrum (solid line). At $(\bar{V} - V_c)/V_c = 0.64$ the shape of the current-noise spectrum has changed considerably, showing additional maxima and minima at high frequencies, which cannot be related to potential-trough transit-times. Since no deviating behaviour of the corresponding ac impedance was found in this high-frequency range, a possible explanation may be that the assumptions for the spectral cross-intensities of the Langevin source-functions do not hold here [13]. Another explanation could be that the additional peaks in the current-noise spectrum result from parametric amplification of subharmonic acoustic waves, as reported by Schulz et al. [10, 11] for GaAs. Indeed these contributions to the current noise, which are associated with subharmonic waves, have been found to become more important with increasing applied voltage. So far we cannot explain why these deviations occur in this particular sample. Similar deviations from the theory were observed for sample s_5.

The arrows in fig. 7 correspond to the resonance frequencies in the ac impedance. With increasing voltage we observe a decrease in the potential-trough transit-time. This effect can be ascribed to electro-acoustic dispersion [14].

4.2. Photoconducting CdS

Fig. 8 shows the spectral current-noise intensity at 10 MHz plotted versus the reduced voltage $(\bar{V} - V_c)/V_c$ for the photoconducting sample p_1 at two different values of the conductivity. Note that $\sigma = 0.023\ \Omega^{-1}\,m^{-1}$ corresponds to the dark-conductivity. Marked deviations from a quadratic relationship are observed. At $(\bar{V} - V_c)/V_c \approx 1$ even a local minimum in the current noise is observed at both conductivities. Fig. 9 shows corresponding results for sample p_2. The value of $\sigma = 0.55\ \Omega^{-1}\,m^{-1}$ corresponds to the dark-conductivity. The behaviour of the photoconducting samples in figs. 8 and 9 is similar to that of the semiconducting samples in fig. 3. It is concluded that in general the current noise at a fixed frequency is not proportional to $(\bar{V} - V_c)^2$, which is contrary to the predictions in [6] and

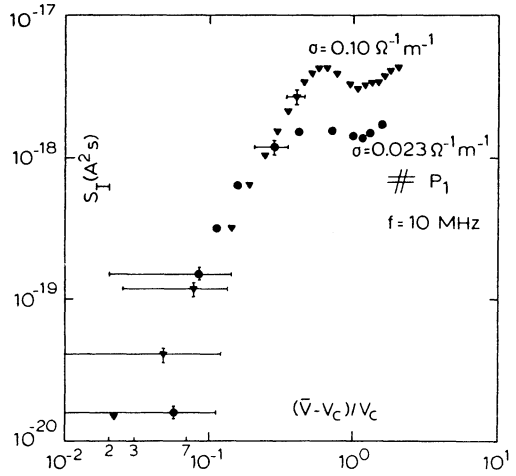

Fig. 8. The spectral current-noise intensity at 10 MHz versus $(\bar{V} - V_c)/V_c$ for sample p_1 at two different conductivities (σ). The value of $\sigma = 0.023\ \Omega^{-1}\,m^{-1}$ corresponds to the dark-conductivity.

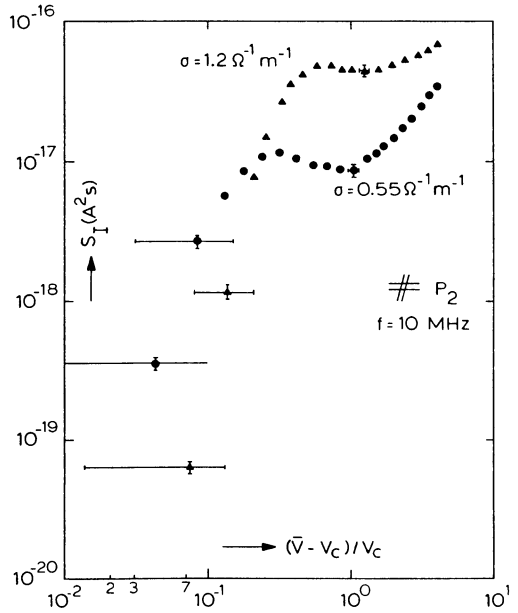

Fig. 9. The spectral current-noise intensity at 10 MHz versus $(\bar{V} - V_c)/V_c$ for sample p_2 at two different conductivities (σ). The value of $\sigma = 0.55\,\Omega^{-1}\,m^{-1}$ corresponds to the dark-conductivity.

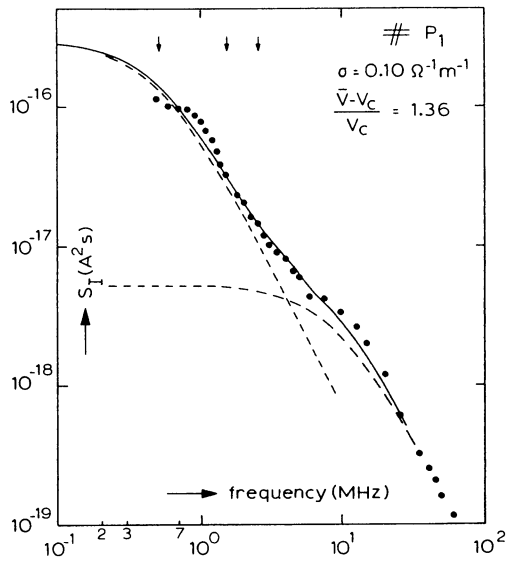

Fig. 10. The spectral current-noise intensity for sample p_1 at $\sigma = 0.10\,\Omega^{-1}\,m^{-1}$ for $(\bar{V} - V_c)/V_c = 1.36$. The solid line has been calculated with eq. (1). The parameters used are listed in table A.1 (appendix). The dashed lines represent the separate contributions of the Lorentzians in eq. (1). The vertical arrows correspond to maxima in the ac impedance.

[12]. The more complicated voltage dependence we found might be connected with the voltage dependence of the parameters τ_1, τ_2, N_1, N_2, v_{g_3}, $\bar{v}_{d_3}$, $\bar{n}_{s_1}$ and $\bar{n}_{s_2}$, according to eq. (1).

Fig. 10 shows a current-noise spectrum for sample p_1. The solid line was calculated with the fitting procedure discussed in section 4.1. Thus, the value of τ_1 that we used was obtained from the corresponding ac-impedance data. The dashed lines represent the separate contributions of the two Lorentzians in eq. (1), and the arrows correspond to the maxima in the ac impedance. We found that the numbers of electrons per trough N_1 and N_2 are of the same order of magnitude as those obtained for semiconductors. For details we refer to table A.1 (appendix).

Fig. 11 shows current-noise spectra for sample p_2 at two different applied voltages. The solid lines represent hand-fit single Lorentzian curves. The parameters used are listed in table A.1 (appendix). Again the arrows correspond to maxima in the ac impedance. It is concluded from fig. 11 that in the frequency range con-

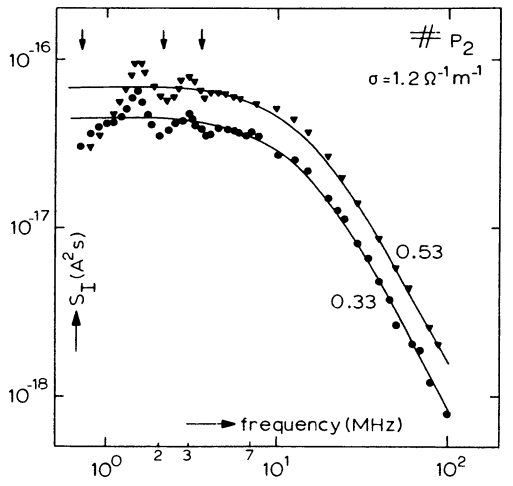

Fig. 11. Current-noise spectra of sample p_2 at $\sigma = 1.2\,\Omega^{-1}\,m^{-1}$ at $(\bar{V} - V_c)/V_c = 0.33$ and 0.53, respectively. The solid lines are hand-fitted single Lorentzian curves. Details are given in table A.1 (appendix). The arrows correspond to maxima in the ac impedance.

sidered the current noise is dominated by the kinetics of the backward-travelling troughs.

Fig. 12 shows two current-noise spectra for sample p_2 at $\sigma = 0.55\,\Omega^{-1}\,m^{-1}$ (dark-conductivity). The transit-time effects are less pronounced and the roll-off frequencies are slightly lower than those in fig. 11.

We conclude that electro-acoustic current noise of photoconducting CdS samples and semiconducting CdS samples is similar. Furthermore it seems that the particular shape of the current-noise spectrum of a certain sample is not predictable. So far we have not succeeded in finding how the parameters occurring in the expression for the current noise depend on the experimental conditions. We conclude, however, that in most cases the current noise apart from transit-time resonances can be described by eq. (1).

4.3. The electron mobility

Several authors [16–18] have reported that the electron mobility in different CdS crystals can differ considerably due to different impurity concentrations and crystal imperfections. The

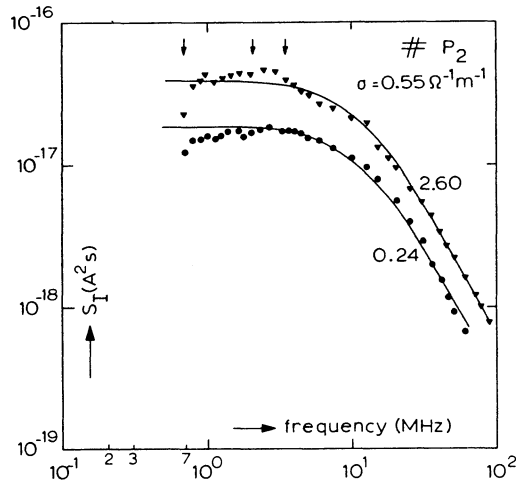

Fig. 12. Current-noise spectra for sample p_2 at $\sigma = 0.55\,\Omega^{-1}\,m^{-1}$ (dark-conductivity) at $(\bar{V} - V_c)/V_c = 0.24$ and 2.60, respectively. The solid lines are hand-fitted single Lorentzians. The parameters used are listed in table A.1 (appendix). The arrows correspond to maxima in the ac impedance.

mobility values for CdS reported in the literature lie between $1.25 \times 10^{-2}\,m^2\,V^{-1}\,s^{-1}$ [17] and $3.88 \times 10^{-2}\,m^2\,V^{-1}\,s^{-1}$ [19] at room temperature. Thus, unfortunately, we cannot rely on the literature to obtain the mobility values for our particular CdS samples, necessary for the calculations. From table I we find that all CdS samples discussed in this paper have different (dark-) conductivities and therefore different impurity concentrations and crystal imperfections. No detailed information about these concentrations and imperfections, and about the possible associated donor-levels and traps was available.

However, the mobility can be obtained from the onset voltage for the electro-acoustic current fluctuations with the help of eq. (3), if the phase velocity $v_s(0)$ of the on-axis waves is known. In our samples only the transverse waves are amplified [14]. When the elastic constants given in [20, 21] were used $v_s(0)$ for transverse waves was found to be $1.77 \times 10^3\,m\,s^{-1}$.

In fig. 13 we have plotted the electron mobilities at room temperature obtained with eq. (3) for the samples discussed in this paper versus the conductivity. The results for the semiconducting samples have been indicated by black dots; the results for the photoconducting samples p_1 and p_2 have been indicated by triangles and squares, respectively. For comparison we have shown the results of Bube et al. [16] obtained from Hall measurements and conductivity measurements on several photoconducting CdS crystals (solid lines). The dashed line represents mobility values obtained by Krischer [18] from ultrasonic amplification measurements.

From fig. 13 we conclude that the electron mobilities obtained from the onset voltage of electro-acoustic current fluctuations are well within the range of mobility values reported in the literature. Furthermore we observe that the mobility data, apart from those for sample p_1, are almost independent of the conductivity, in spite of different concentrations of possible carrier scattering centres. This result indicates that in our samples scattering of electrons by phonons is much more important than impurity scattering.

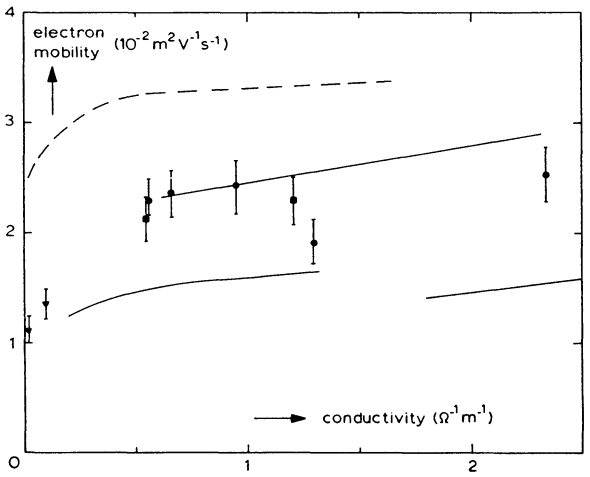

Fig. 13. The electron mobility obtained from the onset voltage of electro-acoustic current fluctuations for the samples discussed in this paper plotted versus the conductivity. Data for the semiconducting samples are indicated by black dots. Data for the photoconducting samples p_1 and p_2 are indicated by triangles and squares respectively. The conductivities $\sigma = 0.02\,\Omega^{-1}\,m^{-1}$ and $\sigma = 0.55\,\Omega^{-1}\,m^{-1}$ correspond to the dark-conductivities of samples p_1 and p_2, respectively. The solid lines represent Hall mobilities of several photoconducting CdS crystals reported in [16]. The dashed line represents mobility data obtained from ultrasonic amplification measurements [18].

From the temperature dependence of the Hall mobility in CdS Pödör et al. [17, 22] concluded that polar optical-phonon scattering is indeed the dominant scattering mechanism at room temperature for conductivities smaller than $50\,\Omega^{-1}\,m^{-1}$.

The relatively low values for the mobility obtained for sample p_1 may be caused by the trapping of electro-acoustically produced space charge in bound-electron states in the forbidden gap. According to White [2] these carrier-trapping effects can be accounted for by multiplying the carrier mobility by a factor f_0, where $0 \leqq f_0 \leqq 1$. Only a fraction f_0 of the electro-acoustically produced space charge is free and contributes to the conductivity. A fraction $(1 - f_0)$ of the space charge is produced by electrons trapped in states in the forbidden gap and is immobile. As the conductivity of sample p_1 is relatively low compared to that of the other samples, a certain number of electron trapping-centres will be empty. Thence, these centres will be able to trap part of the electro-acoustically produced space charge. The mobility data for sample p_1 may thus be interpreted as an apparent mobility given by $f_0\mu_{33}$, where μ_{33} is the real mobility resulting from optical phonon scattering.

Acknowledgements

The author is very grateful to Prof. C.Th.J.

Appendix

Table A.1
Parameter values used in fitting eq. (1) to the experimental current-noise data.

Sample	Fig.	Conductivity ($\Omega^{-1}m^{-1}$)	$\frac{\bar{V} - V_c}{V_c}$	N_1	N_2	$\bar{n}_{s_1}$ ($10^{19}m^{-3}$)	$\bar{n}_{s_2}$ ($10^{19}m^{-3}$)	τ_1 (10^{-7}s)	τ_2 (10^{-8}s)	v_{g_3} ($10^3 ms^{-1}$)
s_2 [a]	4	5.6×10^{-1}	0.36	1.3×10^5	1.6×10^4	5.1	1.1	3.1	1.6	1.66
s_2 [b]	4	5.6×10^{-1}	0.36	6.5×10^4	1.8×10^4	5.1	1.1	3.1	1.6	1.66
s_4	5	6.6×10^{-1}	0.35	7×10^4	3×10^4	5.3	1.3	3.6	1.4	1.62
s_3	6	9.5×10^{-1}	0.94		2×10^4		1.7		8.0	1.68
s_3	6	9.5×10^{-1}	2.96		5×10^3		2.8		5.5	1.68
s_6	7	2.3	0.19		7×10^5		0.28		5.9	1.53
p_1	10	1.0×10^{-1}	1.36	1.6×10^4	1.4×10^4	2.6	0.18	3.3	1.9	1.70
p_2	11	1.2	0.33		1.6×10^5		1.2		1.2	1.60
p_2	11	1.2	0.53		2.2×10^5		1.2		1.1	1.60
p_2 [c]	12	5.5×10^{-1}	0.24		2.3×10^5		0.34		1.3	1.60
p_2 [c]	12	5.5×10^{-1}	2.60		7.7×10^4		0.47		1.4	1.60

[a] Solid line. [b] Dotted line. [c] Dark-conductivity.

Alkemade and Prof. R.J.J. Zijlstra for their critical reading of the manuscript and their valuable suggestions and comments. This work was performed as part of the research programme of the "Stichting voor Fundamenteel Onderzoek der Materie" (FOM) with financial support from the "Nederlandse Organisatie voor Zuiver-Wetenschappelijk Onderzoek" (ZWO).

References

[1] A.R. Hutson, J.H. McFee and D.L. White, Phys. Rev. Lett. 7 (1961) 237.
[2] D.L. White, J. Appl. Phys. 33 (1962) 2547.
[3] K. Blötekjaer and C.F. Quate, Proc. IEEE 52 (1964) 360.
[4] W. Wettling and M. Bruun, Phys. Stat. Sol. 34 (1969) 221.
[5] B.W. Hakki and R.W. Dixon, Appl. Phys. Lett. 14 (1969) 185.
[6] A.R. Moore, J. Appl. Phys. 38 (1967) 2327.
[7] V.I. Baibakov, Sov. Phys.-Semic. 3 (1969) 274.
[8] P.A. Gielen and R.J.J. Zijlstra, Physica 95B (1978) 347.
[9] P.A. Gielen and R.J.J. Zijlstra, Physica 103B (1981) 165.
[10] M. Schulz and B.K. Ridley, Phys. Lett. 29A (1969) 17.
[11] M. Schulz, Sol. St. Comm. 8 (1970) 355.
[12] R.J.J. Zijlstra and P.A. Gielen, Physica 95B (1978) 190.
[13] W. Westera, Physica 113B (1982) 149.
[14] W. Westera, Physica 113B (1982) 284.
[15] J.E. Hill and K.M. van Vliet, Physica 24 (1958) 709.
[16] R.H. Bube and H.E. MacDonald, Phys. Rev. 121 (1961) 473.
[17] B. Pödör, J. Balázs and M. Hársy, Phys. Stat. Sol. (a) 8 (1971) 613.
[18] C. Krischer, Phys. Rev. B 8 (1973) 3908.
[19] J.D. Zook and R.N. Dexter, Phys. Rev. 129 (1963) 1980.
[20] D. Berlincourt, H. Jaffe, and L.R. Shiozawa, Phys. Rev. 129 (1963) 1009.
[21] I.B. Kobiakov, Sol. St. Comm. 35 (1980) 305.
[22] B. Pödör, Act. Phys. Acad. Sci. Hung. 36 (1974) 431.